

Spin-glass state of vortices in $\text{YBa}_2\text{Cu}_3\text{O}_y$ and $\text{La}_{2-x}\text{Sr}_x\text{CuO}_4$ below the metal-to-insulator crossover

J.E. Sonier,^{1,2,*} F.D. Callaghan,¹ Y. Ando,³ R.F. Kiefl,^{2,4} J.H. Brewer,^{2,4} C.V. Kaiser,¹ V. Pacradouni,¹

S.A. Sabok-Sayr,¹ X.F. Sun,³ S. Komiya,³ W.N. Hardy,^{2,4} D.A. Bonn,^{2,4} and R. Liang^{2,4*}

¹*Department of Physics, Simon Fraser University, Burnaby, British Columbia V5A 1S6, Canada*

²*Canadian Institute for Advanced Research, 180 Dundas Street West, Toronto, Ontario M5G 1Z8, Canada*

³*Central Research Institute of Electric Power Industry, Komae, Tokyo 201-8511, Japan*

⁴*Department of Physics and Astronomy, University of British Columbia, Vancouver, British Columbia V6T 1Z1, Canada*

(Dated: November 26, 2018)

Highly disordered magnetism confined to individual weakly interacting vortices is detected by muon spin rotation (μSR) in two different families of high-transition-temperature (T_c) superconductors, but only in samples on the low-doping side of the low-temperature normal state metal-to-insulator crossover (MIC). The results support an extended quantum phase transition (QPT) theory of competing magnetic and superconducting orders that incorporates the coupling between CuO_2 planes. Contrary to what has been inferred from previous experiments, the static magnetism that coexists with superconductivity near the field-induced QPT is not ordered. Our findings unravel the mystery of the MIC and establish that the normal state of high- T_c superconductors is ubiquitously governed by a magnetic quantum critical point (QCP) in the superconducting phase.

PACS numbers: 74.72.-h, 74.25.Ha, 74.25.Qt, 76.75.+i

I. INTRODUCTION

For two decades, arrival at a firm theory for high- T_c superconductivity has been hindered by an incomplete characterization of the phase diagram for cuprate materials. In zero field, μSR ,^{1,2,3,4,5,6} NMR/NQR⁷ and neutron scattering^{8,9} studies show that static (or quasistatic) magnetism coexists with superconductivity in the underdoped regime. Field-induced or enhanced *static magnetic order* has also been clearly detected in underdoped $\text{La}_{2-x}\text{Sr}_x\text{CuO}_4$ (LSCO: x),^{10,11,12} $\text{Pr}_{1-x}\text{LaCe}_x\text{CuO}_4$,^{13,14} and $\text{La}_2\text{CuO}_{4+y}$ ^{15,16} by neutron scattering, and in underdoped $\text{Pr}_{2-x}\text{Ce}_x\text{CuO}_4$ (PCCO),¹⁷ $\text{Pr}_{1-x}\text{LaCe}_x\text{CuO}_4$,¹⁸ and LSCO: x ¹⁹ by μSR . The neutron studies on LSCO: x and $\text{La}_2\text{CuO}_{4+y}$ support a proposed phase diagram by Demler *et al.*²⁰ in which the pure superconductor undergoes a QPT to a phase of coexisting static magnetic and superconducting orders. A similar phase transition compatible with the theory of Ref.²⁰ has also been observed in CeRhIn_5 .²¹ Still the general applicability of this QPT model is questionable, since field-induced static magnetic order has not been established in any of the other hole-doped cuprates.

An important detail in the model of Ref.²⁰ is the assumption that the vortices are two-dimensional (2D). In this case the competing order is stabilized only when there is strong overlap of the 2D vortices within a CuO_2 layer. When this happens long-range magnetic order is established. However, Lake *et al.*²² have shown that the field-induced order in LSCO:0.10 is in fact three-dimensional (3D), implying significant interlayer coupling. Furthermore, a neutron/ μSR study of LSCO:0.10 concluded that the vortices themselves are 3D.²³ Following the work of Ref.²⁰, Kivelson *et al.* showed that competing order can be stabilized about a nearly isolated 3D vortex.²⁴ The field-induced QPT in this extended 3D

model is argued to be to a coexistence phase in which the spatial dependence of the competing order is substantially non-uniform.

Here we show that there is a generic field-induced transition to a coexistence phase where spin-glass-like (SG) magnetism is confined to weakly interacting 3D vortices. The detection of this phase implies that the QPT previously identified in LSCO: x by neutrons scattering is simply a crossover to a situation where competing static magnetism is spatially uniform in the sample. Furthermore, we identify the “true” field-induced QPT as occurring near the critical doping for the low-temperature normal-state MIC that occurs at a non-universal doping concentration in cuprate superconductors. The insulating side of the normal-state MIC is characterized by a $\log(1/T)$ divergence of the in-plane resistivity ρ_{ab} ,^{25,26,27,28,29,30,31,32} but it has also been indirectly identified by electronic thermal conductivity measurements.^{33,34,35}

II. EXPERIMENT

Muon spin rotation/relaxation (μSR) measurements were performed at TRIUMF, Canada on LSCO: x and $\text{YBa}_2\text{Cu}_3\text{O}_y$ (YBCO: y) single crystals on either side of the previously determined critical dopings $x_c \approx 0.16$ (Refs.^{26,33,34}) and $y_c \approx 6.55$ (Ref.³⁵) for the low-temperature MIC. The LSCO: x single crystals were grown by the traveling-solvent floating-zone technique,³⁶ whereas the YBCO: y single crystals were grown by a self-flux method in fabricated BaZrO_3 crucibles.³⁷

The μSR method involves the implantation of nearly 100 % spin polarized positive muons into the sample. Like a tiny bar magnet, the magnetic moment of the muon precesses about the local magnetic field B with an

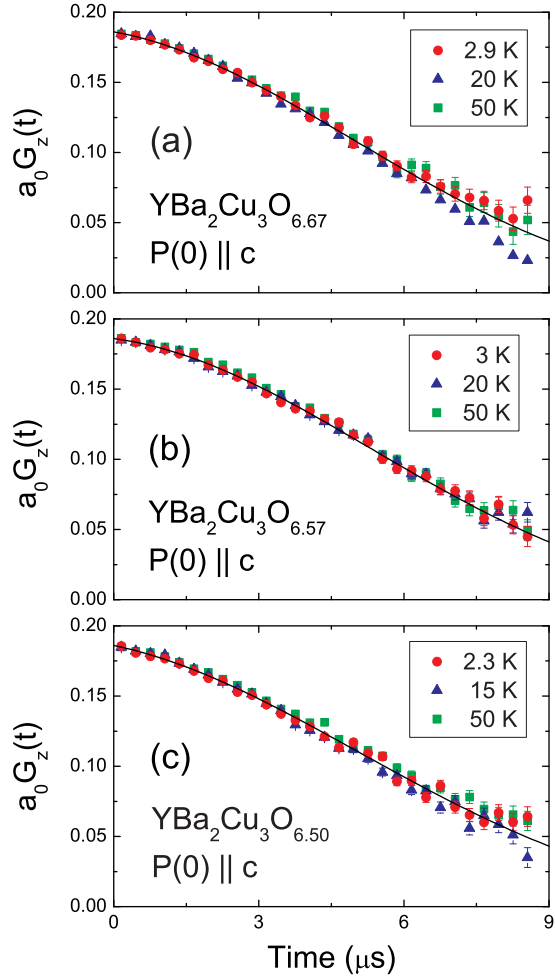


FIG. 1: (Color online) ZF- μ SR time spectra at different temperatures for (a) YBCO:6.67, (b) YBCO:6.57 and (c) YBCO:6.50. In all cases the initial muon spin polarization $\mathbf{P}(0)$ was parallel to the \hat{c} -axis of the single crystals. The solid curves through the data points are fits described in the main text.

angular frequency $\omega_\mu = \gamma_\mu B$, where $\gamma_\mu = 0.0852 \mu\text{s}^{-1} \text{G}^{-1}$ is the muon gyromagnetic ratio. By measuring the time evolution of the polarization of the ensemble of muon spins $P(t)$ via the anisotropic distribution of decay positrons, the internal magnetic field distribution $n(B)$ of the sample is determined.³⁸ As described below, μ SR measurements were first carried out in zero external field to search for *static* electronic moments. The vortex cores were then probed by transverse-field (TF) μ SR, with the applied magnetic field perpendicular to the CuO_2 layers.

III. ZERO-FIELD MEASUREMENTS

Figures 1 and 2 show ZF- μ SR time spectra for some of the samples. Defining the direction of the initial muon

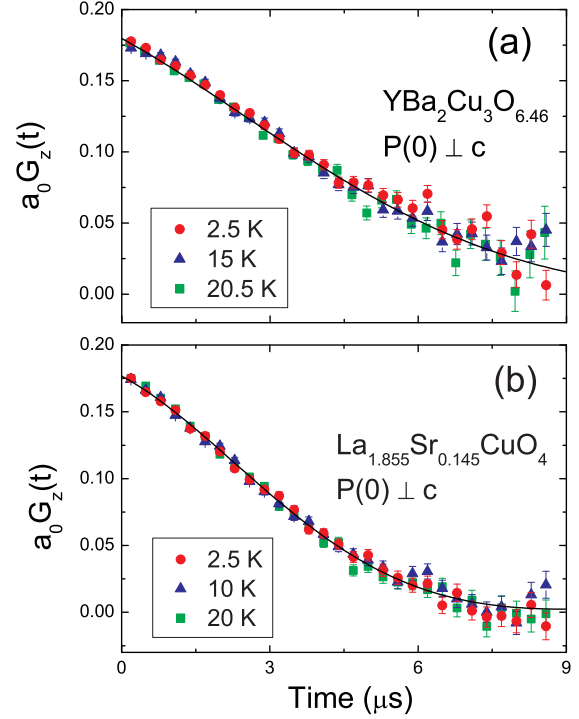


FIG. 2: (Color online) ZF- μ SR time spectra at different temperatures for the lowest doped samples (a) YBCO:6.46, and (b) LSCO:0.145, recorded with the initial muon spin polarization $\mathbf{P}(0)$ perpendicular to the \hat{c} -axis of the single crystals. The solid curves through the data points are fits described in the main text.

spin polarization $\mathbf{P}(0)$ to be parallel to the \hat{z} -axis, the ZF- μ SR or “asymmetry” spectrum has the form

$$A(t) = a_0 P_z(t) = a_0 G_z(t), \quad (1)$$

where a_0 is the initial asymmetry and $G_z(t)$ is a relaxation function. In all cases the spectra are well described by the following ZF relaxation function

$$G_z(t) = G_z^{\text{KT}}(t) \exp(-\lambda t), \quad (2)$$

where

$$G_z^{\text{KT}}(t) = \frac{1}{3} + \frac{2}{3}(1 - \Delta^2 t^2) \exp\left(-\frac{1}{2}\Delta^2 t^2\right), \quad (3)$$

is the static Gaussian Kubo-Toyabe function (KT) typically used to describe relaxation due to nuclear dipole fields, and λ is an additional exponential relaxation rate. In the absence of static or slowly fluctuating electronic moments, the relaxation of the ZF- μ SR signal is caused solely by the nuclear dipoles. In this case the relaxation is expected to be independent of temperature, as observed in Figs. 1 and 2. Fitted values for Δ and λ are given in Table I. The measurements on YBCO:6.46 and LSCO:0.145 were done using a different spectrometer, and with the initial muon spin polarization $\mathbf{P}(0)$

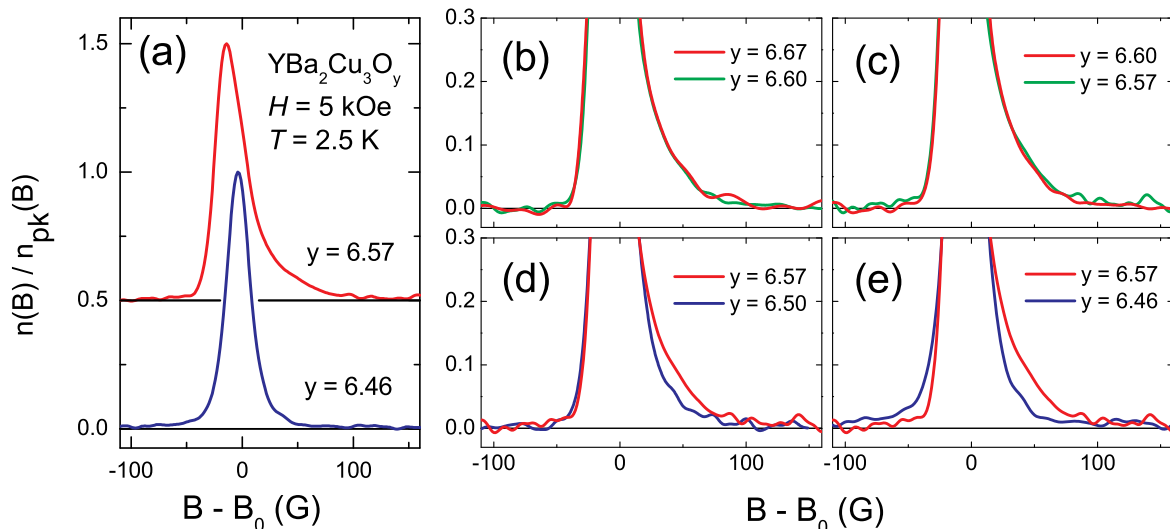


FIG. 3: (Color online) Doping dependence of the μ SR line shapes for $\text{YBa}_2\text{Cu}_3\text{O}_y$ at $H = 5$ kOe and $T = 2.5$ K. (a) Full μ SR line shape for samples above ($y = 6.57$) and below ($y = 6.46$) the critical doping $y_c = 6.55$ for the MIC. (b), (c), (d), (e) Blowups of the ‘tail’ region of the μ SR line shapes above ($y = 6.67, 6.60$ and 6.57) and below ($y = 6.50$ and 6.46) $y_c = 6.55$. For comparison, all line shapes have been normalized as described in the main text.

TABLE I: Results of fits of the ZF- μ SR time spectra to Eq. (2). The fits are shown as solid curves in Figs. 1 and 2.

Sample	Δ (μs^{-1})	λ (μs^{-1})	Polarization
YBCO:6.50	0.1120(3)	0.0381	$\mathbf{P}(0) \parallel \hat{c}$
YBCO:6.57	0.1194(2)	0.0244	$\mathbf{P}(0) \parallel \hat{c}$
YBCO:6.67	0.1207(1)	0.0332	$\mathbf{P}(0) \parallel \hat{c}$
YBCO:6.46	0.1277	0.1044	$\mathbf{P}(0) \perp \hat{c}$
LSCO:0.145	0.195(10)	0.11(2)	$\mathbf{P}(0) \perp \hat{c}$

perpendicular, rather than parallel to the \hat{c} -axis. In this geometry the relaxation rate is larger due to the anisotropy of the muon-nuclear dipole interaction.³⁹ The hole doping dependence of Δ in YBCO: y is explained by a change in the ratio of muons stopping near the O(1) and O(4) oxygen sites.⁴⁰ While there is a residual exponential relaxation rate for all samples, λ is independent of both temperature and hole doping concentration. Thus there is no evidence from the ZF- μ SR spectra for static electronic moments in our samples, which is an essential requirement for establishing the presence of hidden competing magnetic order. We remark that the temperature-independent exponential component may come from the fraction of muons missing the sample and avoiding the background suppression scheme of the spectrometer. Furthermore, the measurements here do not rule out the presence of a weak temperature dependent relaxation rate found in earlier high precision ZF- μ SR measurements of YBCO: y .^{40,41}

IV. TRANSVERSE-FIELD MEASUREMENTS

In a transverse field, the muon spin precesses in a plane perpendicular to the field axis. In this case the asymmetric spectrum is

$$A(t) = a_0 P_x(t) = a_0 G_x(t) \cos(\gamma_\mu B t), \quad (4)$$

where $G_x(t)$ is the transverse muon spin relaxation function and B is the local field at the muon site. In the vortex state the internal magnetic field is spatially inhomogeneous, and the TF- μ SR signal for a perfectly ordered flux-line lattice (FLL) is described by the polarization function

$$P_x(t) = \sum_i \cos[\gamma_\mu B(r_i)t], \quad (5)$$

where the sum is over all sites in the real-space unit cell of the FLL and $B(r_i)$ is the local field at position $r_i = (x_i, y_i)$. A Fourier transform of $P_x(t)$

$$n(B) = \int_0^\infty P_x(t) e^{-i(\gamma_\mu B t)} e^{-\sigma_A^2 t^2 / 2} dB, \quad (6)$$

often called the ‘ μ SR line shape’, provides a fairly accurate visual illustration of the internal magnetic field distribution sensed by the muons. Here $\exp(-\sigma_A^2 t^2 / 2)$ is a Gaussian apodization function used to suppress the ‘ringing’ effect of the finite time range of $P_x(t)$. Figure 3(a) shows a couple of examples of the μ SR line shape for YBCO: y at $H = 5$ kOe and $T = 2.5$ K. The asymmetric line shape for YBCO:6.57 is typical of the field distribution for a 3D FLL.³⁸ Specifically, the ‘high-field’ tail corresponds to the spatial region in and around the vortex cores.

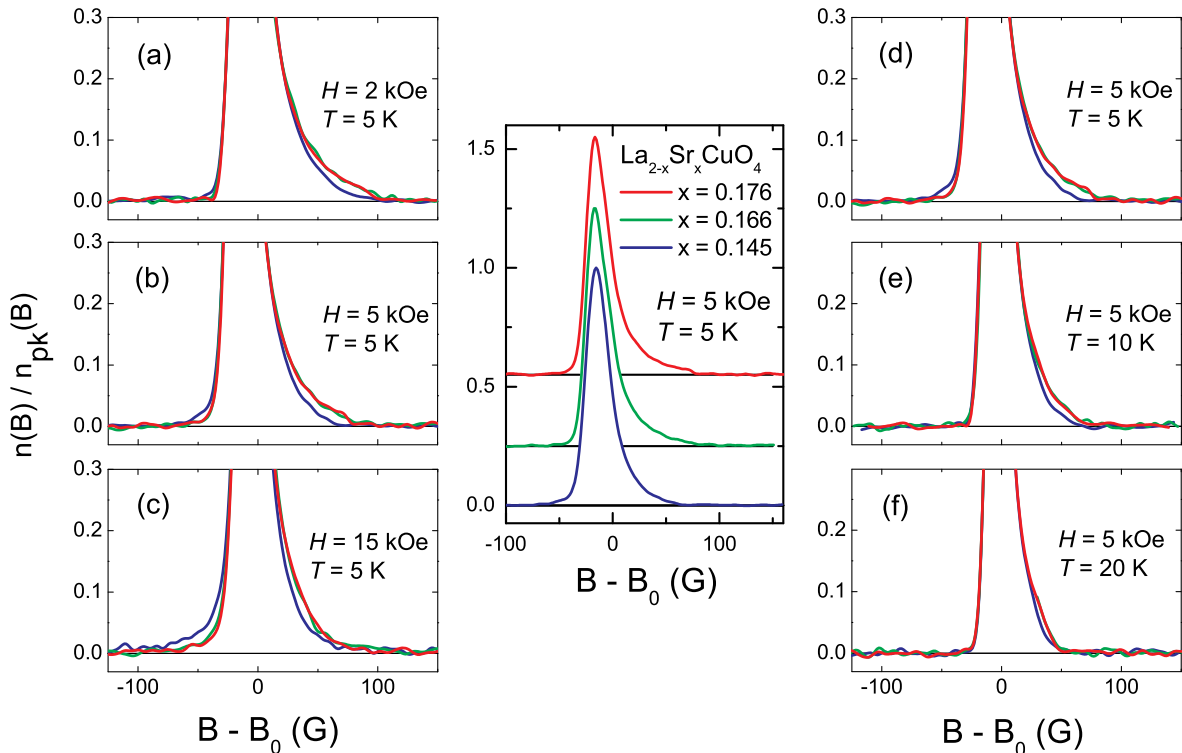


FIG. 4: (Color online) Doping, temperature and magnetic field dependences of the μ SR line shapes for $\text{La}_{2-x}\text{Sr}_x\text{CuO}_4$. The center panel shows the full μ SR line shapes at $H=5$ kOe and $T=5$ K, above ($x=0.176$ and $x=0.166$) and below ($x=0.145$) the critical doping $x_c=0.16$ for the MIC. Panels (a)-(c) show the field dependence of the ‘tail’ regions of the normalized μ SR line shapes. Panels (d)-(f) show the temperature dependence of the ‘tail’ regions of the normalized μ SR line shapes.

Figures 3(b)-(e) show blowups of the ‘tail’ regions of the Fourier transforms of TF- μ SR spectra measured in the vortex state of YBCO: y near the critical doping $y_c \approx 6.55$. For comparison, the line shapes have been normalized to their respective peak amplitude $n_{\text{pk}}(B)$. Furthermore, to account for differences in the in-plane magnetic penetration depth, the widths of the line shapes have been made equivalent by rescaling the horizontal $B-B_0$ axis, where B_0 is the applied magnetic field. Above y_c the μ SR line shapes for $y=6.67$, $y=6.60$ and $y=6.57$ are identical. However, at $y=6.50$ there is a clear *suppression* of the high-field tail, corresponding to the spatial region of the vortex cores. Note that in a previous high-field study of YBCO:6.50 the high-field tail was argued to be enhanced rather than suppressed.⁴² However, this conclusion was based on a comparison of the μ SR line shape to an assumed theoretical curve for $n(B)$. As observed in Fig. 3(e), at $y=6.46$ the suppression of the high-field tail is accompanied by the appearance of a low-field tail.

As shown in Fig. 4, similar differences are observed between the μ SR line shapes of LSCO: x above and below the critical doping $x_c=0.16$ for the MIC. With increasing magnetic field the differences between the tails of the line shapes are enhanced [see Figs 4(a), 4(b) and 4(c)].

On the other hand, with increasing temperature the μ SR line shape of LSCO:0.145 becomes more like that of the samples above $x_c=0.16$ [see Figs. 4(d), 4(e) and 4(f)]. In the next section we explain how field-induced static electronic moments in the samples on the low-doping side of the MIC accounts for both the suppression of the high-field tail and the appearance of a low-field tail.

V. DATA ANALYSIS

While the change in the local magnetic field distribution in the region of the vortex cores is evident from a visual inspection of the μ SR line shapes in Figs. 3 and 4, it is constructive to consider a simple analysis of the TF- μ SR time spectra. Recently we carried out a comprehensive analysis of the μ SR line shape in $y \geq 6.57$ single crystals.⁴⁴ There we showed that the TF- μ SR signal is well described by the polarization function

$$P_x(t) = e^{-\sigma_{\text{eff}}^2 t^2 / 2} \sum_i \cos[\gamma_\mu B(r_i)t], \quad (7)$$

where the Gaussian function $\exp(-\sigma_{\text{eff}}^2 t^2 / 2)$ accounts for additional relaxation due to FLL disorder and nuclear dipole moments, the sum is over all sites in an hexagonal

FLL, and $B(r_i)$ is the following analytical solution of the Ginzburg-Landau equations⁴³

$$B(r_i) = B_0 \sum_{\mathbf{G}} \frac{e^{-i\mathbf{G}\cdot\mathbf{r}_i} F(G)}{\lambda_{ab}^2 G^2}. \quad (8)$$

Here \mathbf{G} are the reciprocal lattice vectors of the FLL, B_0 is the average internal magnetic field, $F(G) = uK_1(u)$ is a cutoff function for the \mathbf{G} sum, $K_1(u)$ is a modified Bessel function, and $u = \sqrt{2}\xi_{ab}G$. The cutoff function $F(G)$ depends on the spatial profile of the superconducting order parameter at the center of the vortex core. Consequently, the parameter ξ_{ab} is a measure of the vortex core size. As explained in Ref.⁴⁴, only the $H \rightarrow 0$ extrapolated value of λ_{ab} is a true measure of the magnetic penetration depth, since at finite H this parameter absorbs deviations of $B(r_i)$ from Eq. (8).

In Ref.⁴² it was assumed that the unusual μ SR line shape of YBCO:6.50 results from static antiferromagnetic order in the vortex cores. However, field-induced static magnetic order has never been observed in YBCO: y by neutron scattering. Furthermore, Khaykovich *et al.* have shown by neutron scattering that static magnetic order occurs in LSCO:0.144 only above $H \approx 30$ kOe.¹² Thus the μ SR line shapes of YBCO:6.46, YBCO:6.50 and LSCO:0.145 presented here for $H \leq 15$ kOe cannot be explained by static magnetic order in and around the vortex cores. Instead we consider the possibility that the weak fields considered here induce disordered static magnetism, which is not ruled out by the neutron scattering experiments. A polarization function that describes the case of disordered static electronic moments in and around the vortex cores is

$$P_x(t) = e^{-\sigma_{\text{eff}}^2 t^2 / 2} \sum_i \exp(-\Lambda e^{-(r_i/\xi_{ab})^2} t) \cos[\gamma_\mu B(r_i)t]. \quad (9)$$

This equation simply says that a muon stopping at position r_i in the FLL experiences a Lorentzian distribution of fields typical of a SG system that results in an exponential decay of $P(t)$. Furthermore, the exponential relaxation rate Λ , and hence the width of the field distribution, is assumed to decrease with increased distance from the center of the vortex core.

Figure 5 shows the real part of the Fourier transform

$$n(B) = \int_0^\infty P_x(t) e^{-i\gamma_\mu B t} e^{-\sigma_\Lambda^2 t^2 / 2} dt, \quad (10)$$

where $P_x(t)$ is calculated from Eq. (9) for the case $\sigma_{\text{eff}} = 0$. The vortex cores are non-magnetic for the case $\Lambda = 0$. When Λ is non-zero the high-field tail of the line shape is suppressed. With increasing Λ the high-field tail is further suppressed, and a low-field tail develops. While the change in the high-field tail is most recognizable, the appearance of the low-field tail depends on the width of the SG Lorentzian field distribution relative to the line width of $n(B)$ for the FLL. For example, in Figs. 5(b) and 5(c) the Lorentzian field distribution of the static

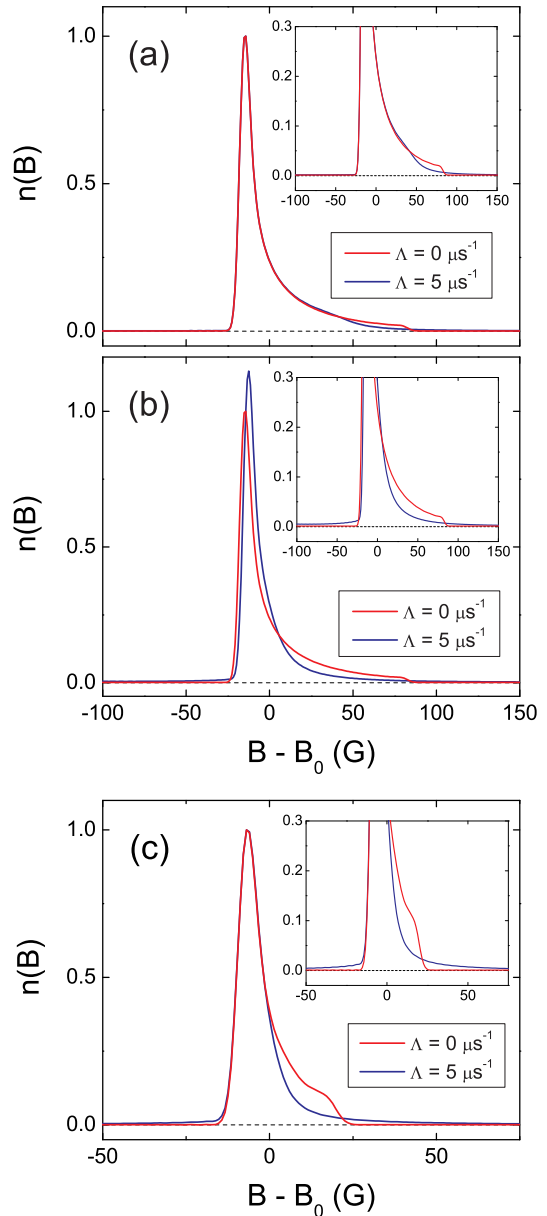


FIG. 5: (Color online) Real part of the Fourier transform of Eq. (9) calculated for two values of Λ ($0 \mu\text{s}^{-1}$ and $5 \mu\text{s}^{-1}$), with $\sigma_{\text{eff}} = 0$ and (a) $\lambda_{ab} = 2000 \text{ \AA}$, $\xi_{ab} = 50 \text{ \AA}$, and $B_0 = 5 \text{ kG}$, (b) $\lambda_{ab} = 2000 \text{ \AA}$, $\xi_{ab} = 100 \text{ \AA}$, and $B_0 = 5 \text{ kG}$, and (c) $\lambda_{ab} = 3000 \text{ \AA}$, $\xi_{ab} = 50 \text{ \AA}$, and $B_0 = 15 \text{ kG}$. All of the Fourier transforms have been generated with a Gaussian apodization of width $\sigma_\Lambda = 0.2 \mu\text{s}^{-1}$. The insets show blowups of the bottom portion of the same Fourier transforms.

magnetism is broad enough to extend beyond the low-field cutoff of the field distribution of the FLL.

Figure 6 shows the temperature dependence of Λ obtained from fits of the TF- μ SR signal to Eq. (9) for some of the samples. Since $\Lambda \approx 0$ for LSCO:0.176 and YBCO:6.60, we conclude that the vortex cores are free

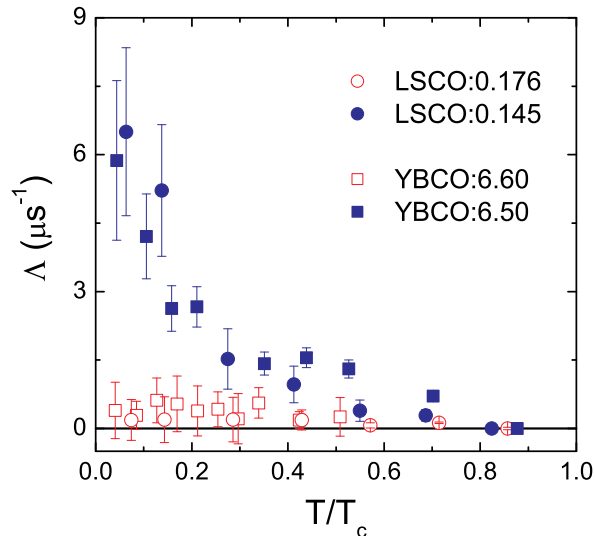


FIG. 6: (Color online) Temperature dependence of Λ from fits of the TF- μ SR time spectra at $H = 5$ kOe to Eq. (9) for LSCO: x and YBCO: y samples above and below the critical dopings $x_c = 0.16$ and $y_c = 6.55$, respectively. At the lowest temperature the fits yield $\lambda_{ab} = 2505(30)$ Å, $\xi_{ab} = 34(3)$ Å, and $\Lambda = 6.5(1.9)$ μs^{-1} for LSCO:0.145, and $\lambda_{ab} = 1950(56)$ Å, $\xi_{ab} = 90(10)$ Å, and $\Lambda = 5.9(1.8)$ μs^{-1} for YBCO:6.50. Note that the vortex core size in YBCO: y at low field is large due to proximity-induced superconductivity on the CuO chain layers.⁴⁴

of static magnetism. On the other hand, the diverging temperature dependence of Λ for LSCO:0.145 and YBCO:6.50 indicates a static broadening of the internal magnetic field distribution associated with the spatial region of the vortex cores. In other words, the increase in Λ with decreasing temperature is consistent with a slowing down of fluctuating Cu spins. Moreover, since the value of Λ does not saturate down to $T = 2.5$ K, the temperature dependence of Λ is consistent with an approach to a second-order magnetic phase transition at $T = 0$ K.

The main changes in the μ SR line shape across the critical doping for the low-temperature MIC are now understandable. From the fitted values of Λ , the half-width at half-maximum of the Lorentzian field distribution assumed in Eq. (9) is approximately ± 70 G in both LSCO:0.145 and YBCO:6.50 at $T = 2.5$ K. For LSCO:0.145 this is broad enough to affect the low-field tail. With increasing field, the density of magnetic vortices increases, while the field inhomogeneity of the FLL decreases. Consequently, at higher magnetic field the static broadening of the μ SR line shape by the magnetism becomes more discernable [see Figs. 4(a)-(c)]. With increasing temperature, the simultaneous loss of the low-field tail and the recovery of the high-field tail of the LSCO:0145 line shape [see Figs. 4(d)-(f)] signifies thermal destruction of the static magnetism in and around the vortex cores.

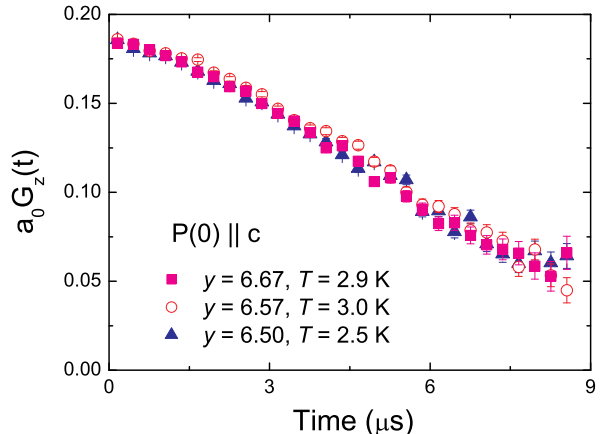


FIG. 7: (Color online) Low-temperature ZF- μ SR time spectra for YBCO: y on either side of the critical doping for the MIC at $y_c = 6.55$.

VI. DISCUSSION

A. Dimensional crossover?

While the onset of SG magnetism in and around the vortex cores fully explains our experimental observations, we note that the change in the μ SR line shape across the MIC is somewhat reminiscent of that observed across the 3D-to-2D vortex crossover field in highly anisotropic $\text{Bi}_{2+x}\text{Sr}_{2-x}\text{CaCu}_2\text{O}_{8+\delta}$ (BSCCO).⁴⁵ In this case random pinning-induced misalignment of the stacked 2D ‘pancake’ vortices that comprise the 3D flux lines in BSSCO, narrows and reduces the asymmetry of the μ SR line shape. The two ingredients necessary for such a crossover are weak coupling between the CuO_2 planes and a source of pinning.

If the vortices in LSCO:0.145 are quasi-2D, the gradual recovery of an asymmetric line shape at higher T that is observed in Fig. 4 signifies thermal depinning of the vortices and a return to an ordered 3D FLL. Such a scenario has been observed in BSCCO.⁴⁶ However, as already mentioned, the vortices in LSCO:0.10 are known to be 3D.^{22,23} Since the effective mass anisotropy $\gamma = \sqrt{m_c^*/m_{ab}^*}$ increases with decreasing hole doping concentration,^{47,48} a novel mechanism that softens the vortex lines at higher doping would be needed to explain the LSCO:0.145 line shapes. As for YBCO: y , mutual inductance measurements show that even severely underdoped samples are quasi-2D only near T_c .⁴⁹ The weak field dependence of the Josephson plasma resonance in YBCO:6.50 at low T is also consistent with 3D vortices.⁵⁰ Thus the extreme vortex anisotropy necessary for a 2D-to-3D crossover does not seem to occur at the hole-doping concentrations investigated here.

Assuming this were not the case, one could imagine an abrupt onset of disorder at the MIC that drives

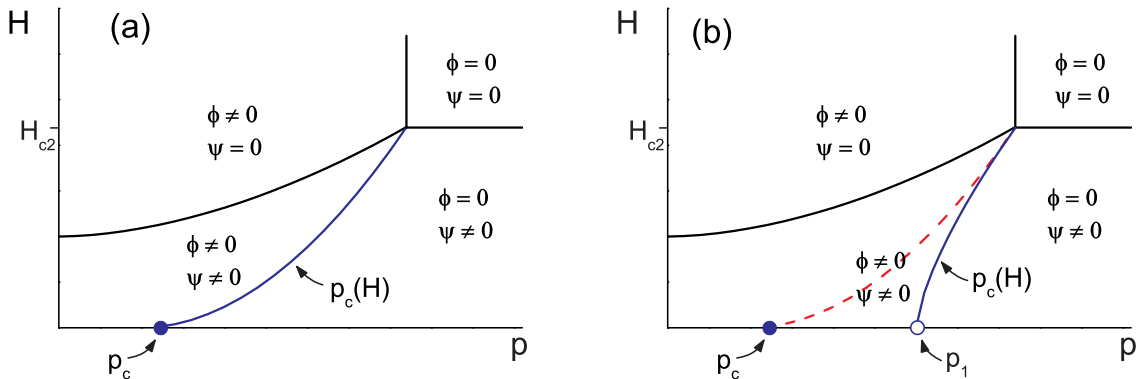


FIG. 8: (Color online) Schematic zero-temperature H versus hole doping concentration p phase diagram for (a) 2D vortices (adapted from figure 1 of Ref.²⁰), and (b) 3D vortices (adapted from figure 1 of Ref.²⁴). Ψ and ϕ denote the expectation values of the superconducting and competing order parameters, respectively. In each panel the solid blue curve is a QPT and the solid blue dot denoted p_c is a QCP. Note that the QPT in (a) becomes a crossover (red dashed curve) in (b). Below the crossover, the competing order is spatially non-uniform. In addition, the $H \rightarrow 0$ extrapolation of the QPT in (b) at p_1 is an ‘avoided’ QCP (open blue circle). Note the Meissner phase is not shown in (a) or (b).

both the logarithmic divergence of the normal-state resistivity and a 3D-to-2D vortex crossover. Since the location of the MIC in LSCO: x has been independently confirmed,^{26,33,34} such pinning would have to be intrinsic to the material. However, disorder in LSCO: x decreases with decreasing Sr doping, and disorder due to excess or deficient oxygen primarily affects the lightly-doped and overdoped regimes, respectively. Likewise, the onset of pinning below the MIC is inconsistent with ortho-II ordering in YBCO:6.50, which reduces random pinning by oxygen disorder and defects. An abrupt redistribution of charge at the MIC is also not supported by our own ZF- μ SR measurements. Previously, ZF- μ SR studies of cuprate superconductors have demonstrated a sensitivity to charge-poor magnetic regions³, and to charge correlations⁴⁰. However, as shown in Fig. 7, the low-temperature ZF- μ SR signal does not change across the MIC.

B. Avoided quantum criticality

Figure 8 shows a comparison of the proposed phase diagrams for competing order in the cuprates for the case of 2D (Ref.²⁰) and 3D (Ref.²⁴) vortices. The major difference is that the inclusion of the interlayer coupling allows the competing phase to be stabilized in nearly isolated vortices, thus altering the position and character of the QPT. There are two key predictions of the extended theory for 3D vortices that are confirmed by our experiments. The first is that there exists a coexistence phase of spatially inhomogeneous competing order. At low fields where the interaction between vortex lines is weaker, we have detected SG magnetism that is local-

ized in and around the vortex cores. This means that the competing order initially stabilized at the QPT is not static magnetic order as previously established, but rather is highly disordered static magnetism. The competing magnetism is characterized by a local order parameter, namely, the mean squared local magnetization. With increasing field, stronger overlap of the magnetism around neighboring vortices may lead to a co-operative bulk crossover to long-range magnetic order, as is apparently the case in La_{1.856}Sr_{0.144}CuO₄.¹² While field-induced static magnetic order has not been detected in YBCO: y , it is worth noting that the MIC occurs at a much lower hole doping concentration ($p_c \approx 0.1$) than in LSCO: x ($p_c = 0.16$). Consequently, very high magnetic fields are likely needed to induce long-range magnetic order in YBCO: y . In contrast, very weak fields were shown to induce magnetic order in PCCO samples that are below the MIC crossover at $p_c \approx 0.16$.¹⁷ This is understandable, since in zero field the superconducting phase of PCCO is in close proximity to the pure antiferromagnetic phase where the competing order parameter is spatially uniform throughout the sample.

Another key prediction of Ref.²⁴ is that there is an ‘avoided’ QCP at $H = 0$, meaning that the QCP lies at a lower doping than the extrapolated $H \rightarrow 0$ value of the field-induced QPT. This is shown in Fig. 8(b). Consistent with this idea, ZF- μ SR studies of pure LSCO: x ,⁴ and YBCO: y ,^{1,6} indicate that the onset temperature for coexisting static magnetism and superconductivity extrapolates to zero below the critical doping for the MIC. While this is well below the doping concentration $p = 0.19$ that Tallon and others^{4,51} have advocated to be a universal QCP in the cuprates, we stress that our study does not prohibit the existence of more than one QCP under

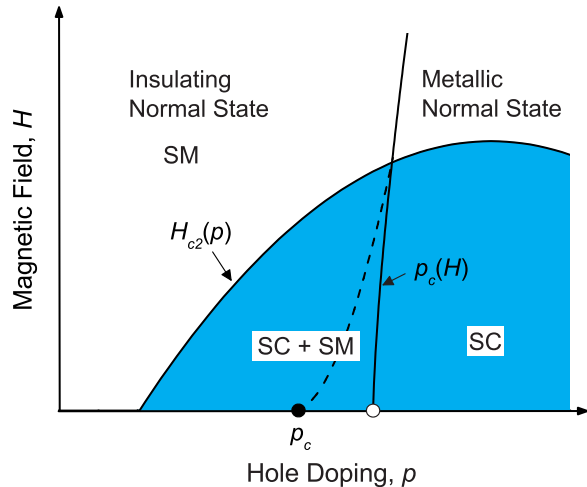


FIG. 9: (Color online) Schematic $T=0$ K phase diagram deduced from this study. The normal and superconducting (SC) phases occur above and below the upper critical field $H_{c2}(p)$, respectively. The solid vertical curve at $p_c(H)$ is a QPT coinciding with the low- T normal-state MIC. Below $H_{c2}(p)$, $p_c(H)$ separates a pure SC phase from a SC phase with coexisting static magnetism (SM). Immediately to the left of $p_c(H)$ the SM is disordered, becoming spatially uniform (and possibly ordered) above the dashed curve. The open circle is the predicted ‘avoided’ QCP,²⁴ whereas the solid circle indicates the ‘true’ QCP at $H=0$.

the superconducting ‘dome’.

VII. CONCLUSIONS

Our experiments clearly demonstrate a change in the internal magnetic field distribution of the vortex state

across the critical doping concentration for the low-temperature MIC in two hole-doped high- T_c superconductors. We have shown that the occurrence of SG magnetism in and around weakly interacting vortices is the most likely source of the observed changes. In Fig. 9 we show a generic zero-temperature phase diagram that is compatible with the present and previous works. We conclude that the strange localization of charge below the MIC stems from competing static magnetism that is stabilized when superconductivity is suppressed by the applied field. While others have hypothesized that magnetism is the cause of the peculiar localization of charge, the experiments here establish that static magnetism not present in zero external field does appear in an applied magnetic field immediately below the critical doping for the MIC. Magnetism plays a prominent role in at least one theory for the MIC. In particular, Marchetti *et al.* have used a spin-charge gauge approach to show that the MIC can arise from a competition between short-range magnetic order and the dissipative motion of the charge carriers.⁵² The experiments here do not rule out the possibility that there are short-range spin correlations in the field-induced magnetism immediately below the MIC.

We thank S.A. Kivelson, R. Greene, B. Lake and E. Demler for informative discussions. J.E. Sonier, J.H. Brewer, R.F. Kiefl, D.A. Bonn, W.N. Hardy and R. Liang acknowledge support from the Canadian Institute for Advanced Research and the Natural Sciences and Engineering Research Council of Canada. Y. Ando acknowledges support from Grant-in-Aid for Science provided by the Japan Society for the Promotion of Science.

* Electronic address: jsonier@sfu.ca

¹ R.F. Kiefl, J.H. Brewer, J. Carolan, P. Dosanjh, W.N. Hardy, R. Kadono, J.R. Kempton, R. Krahn, P. Schleger, B.X. Yang, H. Zhou, G.M. Luke, B. Sternlieb, Y.J. Uemura, W.J. Kossler, X.H. Yu, E.J. Ansaldo, H. Takagi, S. Uchida, and C.L. Seaman, Phys. Rev. Lett. **63**, 2136 (1989).
² A. Weidinger, Ch. Niedermayer, A. Golnik, R. Simon, E. Recknagel, J.I. Budnick, B. Chamberland, and C. Baines, Phys. Rev. Lett. **62**, 102 (1989).
³ Ch. Niedermayer, C. Bernhard, T. Blasius, A. Golnik, A. Moodenbaugh, and J.I. Budnick, Phys. Rev. Lett. **80**, 3843 (1998).
⁴ C. Panagopoulos, J.L. Tallon, B.D. Rainford, T. Xiang, J.R. Cooper, and C.A. Scott, Phys. Rev. B **66**, 064501 (2002).
⁵ A. Kanigal, A. Keren, Y. Eckstein, A. Knizhnik, J.S. Lord, and A. Amato, Phys. Rev. Lett. **88**, 137003 (2002).
⁶ S. Sanna, G. Allodi, G. Concas, A.D. Hillier, and R. De

Renzi, Phys. Rev. Lett. **93**, 207001 (2004).
⁷ M.H. Julien, F. Borsa, P. Carretta, M. Horvatić, C. Berthier, and C.T. Lin, Phys. Rev. Lett. **83**, 604 (1999).
⁸ S. Wakimoto, R.J. Birgeneau, Y.S. Lee, and G. Shirane, Phys. Rev. B **63**, 172501 (2001).
⁹ C. Stock, W.J.L. Buyers, Z. Yamani, C.L. Broholm, J.-H. Chung, Z. Tun, R. Liang, D. Bonn, W.N. Hardy, and R.J. Birgeneau, Phys. Rev. B **73**, 100504(R) (2006).
¹⁰ S. Katano, M. Sato, K. Yamada, T. Suzuki, and T. Fukase, Phys. Rev. B **62**, R14677 (2000).
¹¹ B. Lake, H.M. Ronnow, N.B. Christensen, G. Aeppli, K. Lefmann, D.F. McMorrow, P. Vorderwisch, P. Smeibidl, N. Mangkorntong, T. Sasagawa, M. Nohara, H. Takagi, and T.E. Mason, Nature **415**, 299 (2002).
¹² B. Khaykovich, S. Wakimoto, R.J. Birgeneau, M.A. Kastner, Y.S. Lee, P. Smeibidl, P. Vorderwisch, and K. Yamada, Phys. Rev. B **71**, 220508(R) (2005).
¹³ M. Fujita, M. Matsuda, S. Katano and K. Yamada, Phys. Rev. Lett. **93**, 147003 (2004).

- ¹⁴ H.J. Kang, P. Dai, H.A. Mook, D.N. Argyriou, V. Sikolenko, J.W. Lynn, Y. Kurita, S. Komiya, and Y. Ando, *Phys. Rev. B* **71**, 214512 (2005).
- ¹⁵ B. Khaykovich, Y.S. Lee, R.W. Erwin, S.-H. Lee, S. Wakimoto, K.J. Thomas, M.A. Kastner, and R.J. Birgeneau, *Phys. Rev. B* **66**, 014528 (2002).
- ¹⁶ B. Khaykovich, R.J. Birgeneau, F.C. Chou, R.W. Erwin, M.A. Kastner, S.-H. Lee, Y.S. Lee, P. Smeibidl, P. Vorderwisch, and S. Wakimoto, *Phys. Rev. B* **67**, 054501 (2003).
- ¹⁷ J.E. Sonier, K.F. Poon, G.M. Luke, P. Kyriakou, R.I. Miller, R. Liang, C.R. Wiebe, P. Fournier, and R.L. Greene, *Phys. Rev. Lett.* **91** 147002 (2003).
- ¹⁸ R. Kadono *et al.*, *J. Phys. Soc. Japan* **73** 2944 (2004).
- ¹⁹ A.T. Savici, A. Fukaya, I.M. Gat-Malureanu, T. Ito, P.L. Russo, Y.J. Uemura, C.R. Wiebe, P.P. Kyriakou, G.J. MacDougall, M.T. Rovers, G.M. Luke, K.M. Kojima, M. Goto, S. Uchida, R. Kadono, K. Yamada, S. Tajima, T. Masui, H. Eisaki, N. Kaneko, M. Greven, and G.D. Gu, *Phys. Rev. Lett.* **95**, 157001 (2005).
- ²⁰ E. Demler, S. Sachdev, and Y. Zhang, *Phys. Rev. Lett.* **87**, 067202 (2001).
- ²¹ T. Park, F. Ronning, H.Q. Yuan, M.B. Salamon, R. Movshovich, J. Sarrao, and J.D. Thompson, *Nature* **440** 65 (2006).
- ²² B. Lake, K. Lefmann, N.B. Christensen, G. Aeppli, D.F. McMorrow, H.M. Ronnow, P. Vorderwisch, P. Smeibidl, N. Mangkorntong, T. Sasagawa, M. Nohara, and H. Takagi, *Nature Materials* **4**, 658 (2005).
- ²³ U. Divakar, A.J. Drew, S.L. Lee, R. Gilardi, J. Mesot, F.Y. Ogrin, D. Charalambous, E.M. Forgan, G.I. Menon, N. Momono, M. Oda, C.D. Dewhurst, and C. Baines, *Phys. Rev. Lett.* **92**, 237004 (2004).
- ²⁴ S.A. Kivelson, D.-H. Lee, E. Fradkin, and V. Oganesyan, *Phys. Rev. B* **66**, 144516 (2002).
- ²⁵ Y. Ando, G.S. Boebinger, A. Passner, T. Kimura, and K. Kishio, *Phys. Rev. Lett.* **75**, 4662 (1995).
- ²⁶ G.S. Boebinger, Y. Ando, A. Passner, T. Kimura, M. Okuya, J. Shimoyama, K. Kishio, K. Tamasaku, N. Ichikawa, and S. Uchida, *Phys. Rev. Lett.* **77**, 5417 (1996).
- ²⁷ P. Fournier, P. Mohanty, E. Maiser, S. Darzens, T. Venkatesan, C.J. Lobb, G. Czjzek, R.A. Webb, and R.L. Greene, *Phys. Rev. Lett.* **81**, 4720 (1998).
- ²⁸ S. Ono, Y. Ando, T. Murayama, F.F. Balakirev, J.B. Betts, and G.S. Boebinger, *Phys. Rev. Lett.* **85**, 638 (2000).
- ²⁹ S.Y. Li, W.Q. Mo, X.H. Chen, Y.M. Xiong, C.H. Wang, X.G. Luo, and Z. Sun, *Phys. Rev. B* **65**, 224515 (2002).
- ³⁰ Y. Dagan, M.M. Qazilbash, C.P. Hill, V.N. Kulkarni, and R.L. Greene, *Phys. Rev. Lett.* **92**, 167001 (2004).
- ³¹ S.I. Vedenev and D.K. Maude, *Phys. Rev. B* **70**, 184524 (2004).
- ³² Y. Dagan, M.C. Barr, W.M. Fisher, R. Beck, T. Dhakal, A. Biswas, and R.L. Greene, *Phys. Rev. Lett.* **94**, 057005 (2005).
- ³³ X.F. Sun, S. Komiya, J. Takeya, and Y. Ando, *Phys. Rev. Lett.* **90**, 117004 (2003).
- ³⁴ D.G. Hawthorn, R.W. Hill, C. Proust, F. Ronning, M. Sutherland, E. Boaknin, C. Lupien, M.A. Tanatar, J. Paglione, S. Wakimoto, H. Zhang, L. Taillefer, T. Kimura, M. Nohara, H. Takagi, and N.E. Hussey, *Phys. Rev. Lett.* **90**, 197004 (2003).
- ³⁵ X.F. Sun, K. Segawa, and Y. Ando, *Phys. Rev. Lett.* **93**, 107001 (2004).
- ³⁶ Y. Ando, A.N. Lavrov, S. Komiya, K. Segawa, and X.F. Sun, *Phys. Rev. Lett.* **87**, 017001 (2001).
- ³⁷ R. Liang, D.A. Bonn, and W.N. Hardy, *Physica C* **304**, 105 (1998).
- ³⁸ J.E. Sonier, J.H. Brewer, and R.F. Kiefl, *Rev. Mod. Phys.* **72**, 769 (2000).
- ³⁹ R.F. Kiefl, J.H. Brewer, I. Affleck, J.F. Carolan, P. Dosanjh, W.N. Hardy, T. Hsu, R. Kadono, J.R. Kempton, S.R. Kreitzman, Q. Li, A.H. O'Reilly, T.M. Riseman, P. Schleger, P.C.E. Stamp, H. Zhou, L.P. Le, G.M. Luke, B. Sternlieb, and Y.J. Uemura, *Phys. Rev. Lett.* **64**, 2082 (1990).
- ⁴⁰ J.E. Sonier, J.H. Brewer, R.F. Kiefl, R.H. Heffner, K.F. Poon, S.L. Stubbs, G.D. Morris, R.I. Miller, W.N. Hardy, R. Liang, D.A. Bonn, J.S. Gardner, C.E. Stronach, and N.J. Curro, *Phys. Rev. B* **66**, 134501 (2002).
- ⁴¹ J.E. Sonier, J.H. Brewer, R.F. Kiefl, R.I. Miller, G.D. Morris, C.E. Stronach, J.S. Gardner, S.R. Dunsiger, D.A. Bonn, W.N. Hardy, R. Liang, and R.H. Heffner, *Science* **292**, 1692 (2001).
- ⁴² R.I. Miller, R.F. Kiefl, J.H. Brewer, J.E. Sonier, J. Chakhalian, S. Dunsiger, G.D. Morris, A.N. Price, D.A. Bonn, W.N. Hardy, and R. Liang, *Phys. Rev. Lett.* **88**, 137002 (2002).
- ⁴³ A. Yaouanc, P. Dalmass de Réotier, and E.H. Brandt, *Phys. Rev. B* **55**, 11107 (1997).
- ⁴⁴ J.E. Sonier, A. Sabok-Sayr, F.D. Callaghan, C.V. Kaiser, V. Pacradouni, J.H. Brewer, S.L. Stubbs, W.N. Hardy, D.A. Bonn, R. Liang, and W.A. Atkinson, submitted to *Phys. Rev. B*.
- ⁴⁵ S.L. Lee, P. Zimmermann, H. Keller, M. Warden, I.M. Savić, R. Schauwecker, D. Zech, R. Cubitt, E.M. Forgan, P.H. Kes, T.W. Li, A.A. Menovsky, and Z. Tarnawski, *Phys. Rev. Lett.* **71**, 3862 (1993).
- ⁴⁶ E.M. Forgan, M.T. Wylie, S. Lloyd, S.L. Lee, and R. Cubitt, *Czech. J. Phys.* **46**-suppl. S3, 1571 (1996).
- ⁴⁷ Y. Nakamura and S. Uchida, *Phys. Rev. B* **47**, 8369 (1993).
- ⁴⁸ K. Takenaka, K. Mizuhashi, H.T. Takagi, and S. Uchida, *Phys. Rev. B* **50**, 6534 (1994).
- ⁴⁹ Y. Zuev, M.S. Kim and T.R. Lemberger, *Phys. Rev. Lett.* **95**, 137002 (2005).
- ⁵⁰ D. Dulić, S.J. Hak, D. van der Marel, W.N. Hardy, A.E. Koshelev, R. Liang, D.A. Bonn, and B.A. Willemssen, *Phys. Rev. Lett.* **86**, 4660 (2001).
- ⁵¹ J.L. Tallon, and J.W. Loram, *Physica C* **349**, 53 (2001).
- ⁵² P.A. Marchetti, Z.-B. Su, and L. Yu, *Phys. Rev. Lett.* **86**, 3831 (2001); *ibid* *J. Phys.: Condens. Matter* **19** 125212 (2007).